Supporting Information for "The impact of reservoir construction and changes in land use and climate on ecosystem services in a large Mediterranean catchment"

J.P.C. Eekhout[1], C. Boix-Fayos[1], P. Pérez-Cutillas[2], and J. de Vente[1]

[1]Soil and Water Conservation Research Group, CEBAS-CSIC, Spanish Research Council, Campus de Espinardo 30100, P.O. Box 164, Murcia, Spain
[2]University of Murcia, Department of Geography, Murcia, Spain

Correspondence: Joris Eekhout (joriseekhout@gmail.com)

Contents of this file

Supplementary Material & Methods

Model calibration

Model calibration and validation were performed in a headwater subcatchment (Fuensanta) that is not affected by water extractions for irrigation (696 km^2; Figure 1b). To prevent overfitting and achieve most realistic model calibration we set most of the potential calibration parameters at literature values and maintained the other parameters within reasonable physical limits of the parameter domain. Calibration and validation were performed for the periods 2001-2010 and 1987-2000, respectively. These periods were chosen such that we could make best use of the limited available data, i.e. daily discharge, precipitation, temperature and NDVI images. Daily discharge time series were used to determine model performance. Data were obtained from the Segura River Basin Agency for the Fuensanta reservoir (Figure 1b). We only considered the discharge originating from the Fuensanta subcatchment, by subtracting the discharge from the upstream located subcatchments, both for the observed and the simulated time series. The calibration procedure consisted of two steps. First, we optimized the water balance by comparing the observed and simulated discharge sum (percent bias). We adjusted model parameters related to the soil hydraulic properties and the thickness of the soil (Table S2) to optimize the percent bias of the discharge. In the second step we optimized the Kling-Gupta model efficiency (KGE; *Gupta et al.*, 2009) by adjusting model parameters from the routing module and the infiltration excess surface runoff equation (Table S2). In this step we applied the SPOTPY calibration package (*Houska et al.*, 2015), using the Simulated Annealing algorithm to optimize the KGE. The calibration resulted in a KGE of 0.62 and the validation in a KGE of 0.58 for daily discharge (Figure S2).

The reservoir module was calibrated separately and includes two parameters (k_r and b), which were optimized for KGE for the 18 reservoirs for which storage and outflow observations were available (Table S3). The median values of the optimized parameters were assigned to the remainder of the reservoirs, i.e. $k_r = 0.12$ and $b = 1.97$.

The soil erosion module was calibrated in two large subcatchments (5218 km^2; Figure 1b) for the period 2001–2010 and validated for the period 1981–2000 using plot-scale soil loss data for the Mediterranean region (*Maetens et al.*, 2012). We determined the annual unit soil loss (SLu), which is soil loss corrected for plot length and slope gradient. In the calibration procedure, the model parameters were adjusted such that the average soil loss per land use class was within 1% of the literature values (Table S5). We used the land covered by tree crops as a baseline, for which we assume to have negligible ground cover due to frequent ploughing, hence, land use-specific model parameters do not affect their soil loss. For the land covered by tree crops, we calibrated two model parameters, i.e. the detachability of the soil by raindrop impact (K) and the detachability of the soil by runoff (DR). Then, we calibrated the other land use classes with ground cover (GC), stem diameter (D) and stem density (NV). Table S4 shows the model parameters per land use class.

The sediment transport model was calibrated with reservoir sedimentation data from 6 reservoirs (Figure 1b; *Avendaño-Salas et al.*, 1997) for the period 2001-2010 and validated for the period 1981-2000. The calibration focussed on two model parameters, i.e. β and γ. Calibration resulted in optimized values of $\beta = 1.175$ and $\gamma = 0.425$, yielding an optimized value for KGE of 0.89 for the calibration period and a KGE of 0.57 for the validation period (Table S6).

Inter- and intra-annual NDVI

The inter-annual variability was determined based on a log-linear relationship between the annual precipitation sum, annual average temperature, annual maximum temperature and annual average NDVI for each of the 19 landuse classes for the period 2000-2012:

$$\begin{aligned} NDVI_{\text{year}} =& \beta_0 + \log(P_{\text{year}})\beta_1 + \log(P_{\text{year-1}})\beta_2 + \log(Tavg_{\text{year}})\beta_3 \\ &+ \log(Tavg_{\text{year-1}})\beta_4 + \log(Tmax_{\text{year}})\beta_5 + \log(Tmax_{\text{year-1}})\beta_6 \end{aligned} \tag{S1}$$

Where $NDVI$ is the annual average NDVI, P the annual precipitation sum, $Tavg$ the annual average temperature, $Tmax$ the annual maximum temperature, and β_{0-6} coefficients of the log-linear regression model. We used the annual climate indices of two years, the current year (X_{year}) and the previous year ($X_{\text{year-1}}$), to account for the climate lag that may influence the vegetation development. A stepwise model selection procedure was applied for each of the 19 landuse classes, selecting the best combination of variables from Eq. S1 with the lowest AIC (Akaike Information Criterion) in R (version 3.4.0), using the stepAIC algorithm from the MASS package (*Venables and Ripley*, 2002).

The intra-annual variability was obtained from the long-term average bi-monthly (16 day) NDVI for the period 2000-2012. To account for land use change, we aggregated the intra-annual variability per land use class based on the land use map of 2001, hereby obtaining the average NDVI per land use class. Then we applied the aggregated NDVI values per land use class to all land use maps used in this study.

Plant water stress

Plant water stress is an indicator of the amount of stress plants experience and ranges between 0 (no stress) and 1 (fully stressed). Plant water stress is determined by comparing the soil moisture content with the plant-specific soil moisture content from which stress starts to occur (adapted from *Porporato et al.*, 2001)):

$$\text{PWS} = \frac{\theta_{\text{PWS}} - \theta(t)}{\theta_{\text{PWS}} - \theta_{\text{PWP}}} \tag{S2}$$

with PWS the dimensionless plant water stress, $\theta(t)$ the soil moisture content at timestep t, θ_{PWS} the plant and soil specific soil moisture content from which plant water stress starts to occur and θ_{PWP} the soil moisture content at permanent wilting point. PWS equals zero when $\theta(t) > \theta_{\text{PWP}}$, where θ_{PWS} is determined by (adapted from *Allen et al.*, 1998):

$$\theta_{\text{PWS}} = \theta_{\text{FC}} - d(\theta_{\text{FC}} - \theta_{\text{PWP}}) \tag{S3}$$

with θ_{FC} the soil moisture content at field capacity, and d the depletion fraction. The plant specific depletion fraction is a function of the potential evapotranspiration (*Allen et al.*, 1998):

$$d = d_{\text{tab}} + 0.04(5 - ET_{\text{P}}) \tag{S4}$$

with d_{tab} the tabular value of the depletion fraction and ET_{P} the potential evapotranspiration obtained from the hydrological model. We obtained values for d_{tab} from *Allen et al.* (1998).

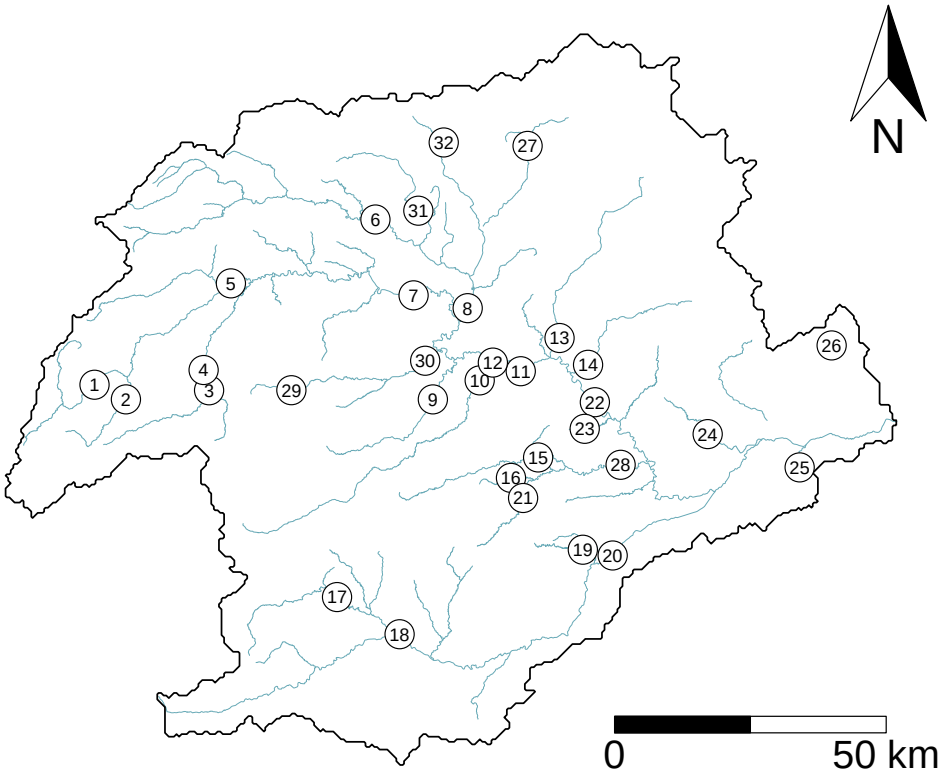

Figure S1. Locations of the 32 reservoirs in the study area. The numbers indicate the reservoir ID.

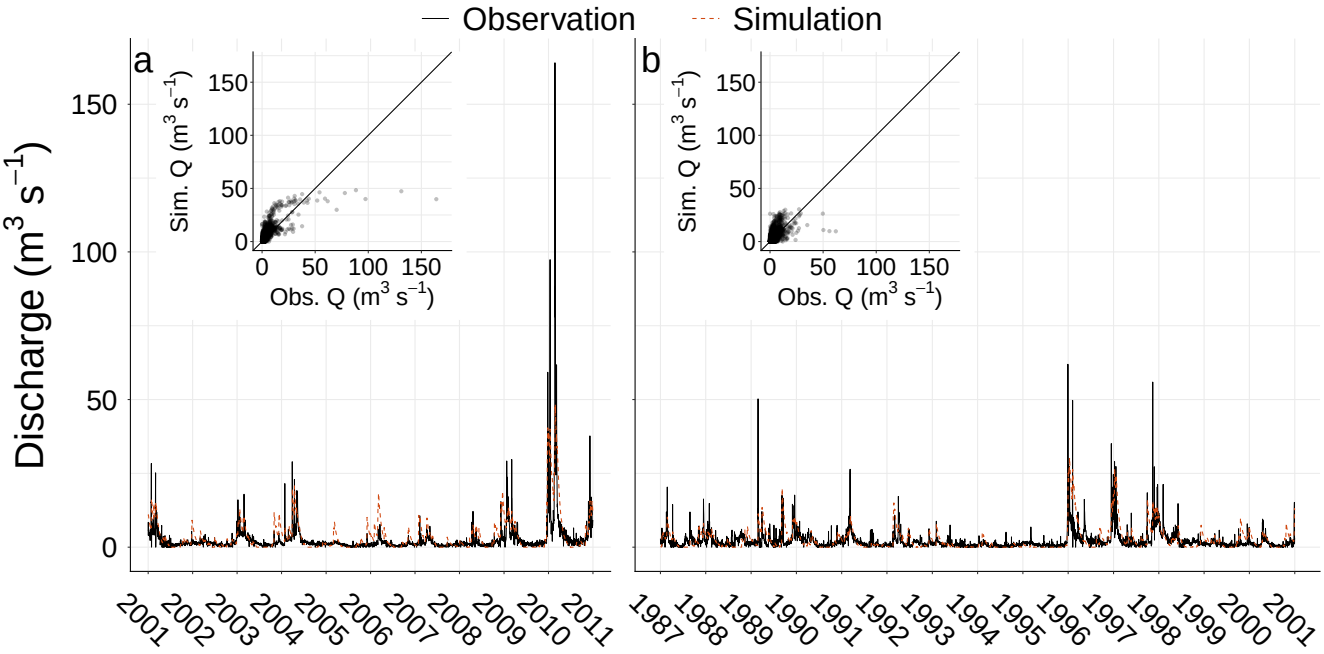

Figure S2. Discharge time series for the calibration (a) and validation period (b). The solid line correspond to the observed time series and the dashed orange line corresponds to the simulated time series. The small insets show the offset between observed and simulated discharge.

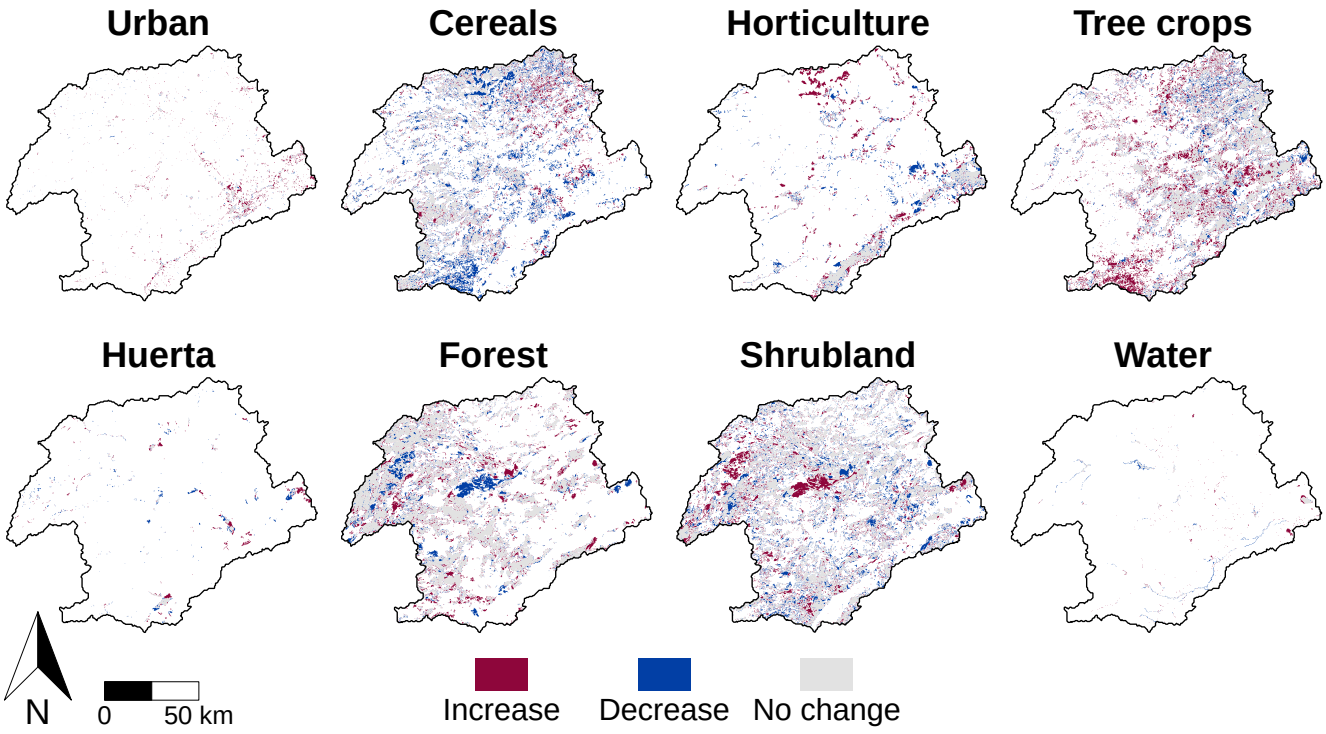

Figure S3. Land use change per land use class, where red indicates an increase, blue a decrease and grey no change.

Table S1. Characteristics of the 32 reservoirs in the Segura River catchment, which include the name, the year of construction, the capacity (Hm^3) and the main use. The ID corresponds to the reservoir locations of Figure S1.

ID	Name	Construction (yr)	Capacity (Hm^3)	Use
17	Valdeinfierno	1806	13	Irrigation and flood control
18	Puentes	1881	26	Irrigation and flood control
10	Alfonso XIII	1916	22	Irrigation and flood control
6	Talave	1918	35	Irrigation and flood control
12	Almadens	1925	0.2	Hydroelectricity
15	La Cierva	1929	7	Irrigation and flood control
5	Fuensanta	1933	210	Irrigation and flood control
1	Anchuricas	1955	6	Hydroelectricity
2	La Vieja	1955	1	Hydroelectricity
4	Taibilla-Toma	1955	1	Drinking water
7	Cenajo	1960	437	Irrigation and flood control
8	Camarillas	1960	36	Irrigation and flood control
24	Santomera	1967	26	Flood control
9	Argos	1974	10	Irrigation and flood control
22	Ojos	1978	1	Irrigation water
3	Taibilla	1979	9	Drinking water
23	Mayes	1980	2	Irrigation water
25	La Pedrera	1985	246	Irrigation water
26	Crevillente	1985	13	Irrigation water
14	Moro	1989	6	Flood control
11	Carcabo	1992	3	Flood control
13	Judío	1992	9	Flood control
16	Noña Ana	1993	3	Flood control
21	Pliego	1993	10	Flood control
19	Algeciras	1995	45	Irrigation and flood control
27	Bayco u Ortigosa	1997	9	Flood control
20	José Bautista Matín	1999	6	Flood control
31	Boquerón	1999	13	Flood control
28	Rodeos	2000	14	Flood control
32	Charcos	2001	4	Flood control
29	Risca	2002	2	Flood control
30	Moratalla	2002	5	Flood control

Table S2. Overview of the parameters that were used to calibrate the hydrological model.

Acronym	Description	Units	Calibrated value	Parameter range
SubDepthFlat	Thickness of the subsoil	mm	500	0-2000
RootFieldFrac	Fraction of the field capacity (rootzone)	-	1.37	0-2
RootDryFrac	Fraction of the permanent wilting point (rootzone)	-	0	0-2
Alpha	Fraction of daily rainfall that occurs in the hour with the highest intensity	-	0.993	0-1
Labda_infil	Infiltration excess parameter	-	0.679	0-1
kx	Flow recession coefficient	-	0.9614	0-0.999

Table S3. Calibrated parameter values and model efficiency of the reservoir module, which is based on the formulation proposed by *Hanasaki et al.* (2006). In the current model, the fixed exponent of 1.5 is replaced by parameter b. The ID corresponds to the reservoir locations of Figure S1.

ID	Name	kr	b	KGE
1	Anchuricas	0.06	4.42	-0.02
2	La Vieja	1.12	1.41	-0.17
3	Taibilla	0.12	3.58	0.03
5	Fuensanta	0.05	0.50	0.61
6	Talave	0.19	0.51	0.30
7	Cenajo	0.07	1.98	0.06
8	Camarillas	0.18	0.51	0.24
9	Argos	0.02	3.79	0.38
10	Alfonso XIII	0.10	1.97	0.34
15	La Cierva	0.08	2.74	-0.08
17	Valdeinfierno	1.10	1.90	0.00
18	Puentes	0.20	0.98	0.13
19	Algeciras	0.80	2.67	0.01
22	Ojos	0.07	2.32	-0.01
23	Mayes	0.72	1.27	0.18
24	Santomera	0.72	2.67	0.25
25	La Pedrera	0.07	3.66	-0.10
26	Crevillente	0.02	3.78	0.05
	Other reservoirs	0.12	1.97	

Table S4. Calibration parameters of the soil erosion module and their values per land use class, with NV the stem density (stems m^{-2}), D the stem diameter (m) and GC the ground cover fraction (-).

Land use class	NV (stems m^{-2})	D (m)	GC (-)
Cereals	400	0.0225	0.2
Horticulture	6.25	0.338	0.71
Tree crops	n/a	n/a	< 0.01
Huerta	500	0.01	0.38
Forest	n/a	n/a	0.639
Shrubland	n/a	n/a	0.697
Urban/water	0	0	1

Table S5. Hillslope erosion results of the calibration and validation of the soil erosion model (Mg km^{-2} yr^{-1}). The results are compared with literature values obtained from *Maetens et al.* (2012).

Land use class	Calibration	Validation	*Maetens et al.* (2012)
Cereals	229.7	218.8	230
Horticulture	229.3	241.2	230
Tree crops	299.9	275.4	300
Huerta	229.1	237.1	230
Forest	40.3	39.1	40
Shrubland	29.8	28.0	30
Urban/water	0	0	n.a.

Table S6. Sediment yield of the calibration and validation of the sediment transport model (Gg yr^{-1}). Results are compared with observed sediment yield values obtained from *Avendaño-Salas et al.* (1997). The ID corresponds to the reservoir locations of Figure S1.

ID	Reservoir	Calibration	Validation	Observations
17	Valdeinfierno	55	49	155
18	Puentes	193	148	191
1	Anchuricas	105	87	87
5	Fuensanta	436	286	456
7	Cenajo	279	231	231
3	Taibilla	120	90	130

Table S7. Land cover (km^2) per land use class, specified for the two land use maps (1977 and 2001) for the Segura River catchment, accompanied by the percentage in parenthesis. The last column shows the change in land cover per land use class (km^2).

Land use class	Land cover (km^2)				Change (km^2)
	1977		2001		
Urban	145.4	(0.9%)	289.6	(1.8%)	144.2
Cereals	3188.9	(20.0%)	2311.3	(14.5%)	-877.6
Horticulture	867.7	(5.4%)	911.4	(5.7%)	43.7
Tree crops	3056.6	(19.2%)	3714.8	(23.3%)	658.2
Huerta	135.8	(0.9%)	149.3	(0.9%)	13.5
Forest	3910.3	(24.5%)	4043.2	(25.3%)	132.9
Shrubland	4556.0	(28.6%)	4443.1	(27.8%)	-112.9
Water	94.4	(0.6%)	92.4	(0.6%)	-2.0

Table S8. Change in the catchment-average climate signal for the Segura River catchment between the periods 1971-1990 and 1991-2010, with change in annual precipitation sum (mm), extreme precipitation (mm) and average temperature (°C). Extreme precipitation is determined with the PCI (*Martin-Vide*, 2004).

	Precipitation sum (mm)	Extreme precipitation (mm)	Average temperature (°C)
1971-1990	402.2	18.3	14.8
1991-2010	376.2	17.5	15.2
Change	-26.0 (-6.5%)	-0.73 (-4.0%)	0.37
	ES = 0.15	ES = 0.40	ES = 0.18

Table S9. Change in ecosystem services indicators as a result of land use change processes, i.e. reforestation, agricultural intensification and urban expansion. Runoff (mm), plant water stress (PWS; -) and hillslope erosion (Mg km^{-2} yr^{-1}) are averaged over the area where forest (for reforestation), tree crops and horticulture (for agricultural intensification), and urban (for urban expansion) land uses increased, respectively (see also Figure S3). The effect size was obtained considering all grid cells in the three respective areas.

LUC process	Runoff (mm)	PWS (-)	Hillslope erosion (Mg km^{-2} yr^{-1})
Reforestation	-31.98 (-22.4%)	0.04 (6.8%)	-23.44 (-78.3%)
	ES = 0.30	ES = 0.37	ES = 0.04
Agricultural	3.87 (4.5%)	0.03 (4.3%)	13.18 (44.6%)
intensification	ES = 0.11	ES = 0.38	ES = 0.05
Urban	143.64 (170.0%)	0.19 (23.6%)	-25.65 (-99.7%)
expansion	ES = 2.24	ES = 2.98	ES = 0.22

References

Allen, R. G., L. Pereira, D. Raes, and M. Smith, Crop evapotranspiration: Guidelines for computing crop requirements, *Tech. Rep. 56*, FAO, https://doi.org/10.1016/j.eja.2010.12.001, 1998.

Avendaño-Salas, C., E. Sanz-Montero, R. Cobo-Rayán, and J. L. Gómez-Montaña, Capacity Situation in Spanish Reservoirs, in *ICOLD, Proceedings of the 19th International Symposium on Large Dams*, pp. 849–862, Florence, 1997.

Gupta, H. V., H. Kling, K. K. Yilmaz, and G. F. Martinez, Decomposition of the mean squared error and NSE performance criteria: Implications for improving hydrological modelling, *Journal of Hydrology*, *377*(1-2), 80–91, https://doi.org/10.1016/j.jhydrol.2009.08.003, 2009.

Hanasaki, N., S. Kanae, and T. Oki, A reservoir operation scheme for global river routing models, *Journal of Hydrology*, *327*(1-2), 22–41, https://doi.org/10.1016/j.jhydrol.2005.11.011, 2006.

Houska, T., P. Kraft, A. Chamorro-Chavez, and L. Breuer, SPOTting model parameters using a ready-made python package, *PLoS ONE*, *10*(12), 1–22, https://doi.org/10.1371/journal.pone.0145180, 2015.

Maetens, W., M. Vanmaercke, J. Poesen, B. Jankauskas, G. Jankauskiene, and I. Ionita, Effects of land use on annual runoff and soil loss in Europe and the Mediterranean: A meta-analysis of plot data, *Progress in Physical Geography*, *36*(5), 599–653, https://doi.org/10.1177/0309133312451303, 2012.

Martin-Vide, J., Spatial distribution of a daily precipitation concentration index in peninsular Spain, *International Journal of Climatology*, *24*(8), 959–971, https://doi.org/10.1002/joc.1030, 2004.

Porporato, A., F. Laio, L. Ridolfi, and I. Rodriguez-Iturbe, Plants in water-controlled ecosystems: active role in hydrologic processes and response to water stress, *Advances in Water Resources*, *24*(7), 725–744, https://doi.org/10.1016/S0309-1708(01)00006-9, 2001.

Venables, W. N., and B. D. Ripley, *Modern Applied Statistics with S*, fourth edi ed., Springer, New York, 2002.